Loss of postnatal quiescence of neural stem cells through mTOR activation upon genetic removal of cysteine string protein-α

Jose L. Nieto-González[a,b,c,1,2], Leonardo Gómez-Sánchez[a,b,c,1], Fabiola Mavillard[a,b,c], Pedro Linares-Clemente[a,b,c], María C. Rivero[a,b,c], Marina Valenzuela-Villatoro[a,b,c], José L. Muñoz-Bravo[a,b,c], Ricardo Pardal[a,b,c], and Rafael Fernández-Chacón[a,b,c,2]

[a]Instituto de Biomedicina de Sevilla (IBiS), Hospital Universitario Virgen del Rocío/Consejo Superior de Investigaciones Científicas/Universidad de Sevilla, 41013 Sevilla, Spain; [b]Departamento de Fisiología Médica y Biofísica, Universidad de Sevilla, 41009 Sevilla, Spain; and [c]Centro Investigación Biomédica en Red Enfermedades Neurodegenerativas, 41013 Sevilla, Spain

Edited by Thomas C. Südhof, Stanford University School of Medicine, Stanford, CA, and approved March 4, 2019 (received for review October 9, 2018)

Neural stem cells continuously generate newborn neurons that integrate into and modify neural circuitry in the adult hippocampus. The molecular mechanisms that regulate or perturb neural stem cell proliferation and differentiation, however, remain poorly understood. Here, we have found that mouse hippocampal radial glia-like (RGL) neural stem cells express the synaptic cochaperone cysteine string protein-α (CSP-α). Remarkably, in CSP-α knockout mice, RGL stem cells lose quiescence postnatally and enter into a high-proliferation regime that increases the production of neural intermediate progenitor cells, thereby exhausting the hippocampal neural stem cell pool. In cell culture, stem cells in hippocampal neurospheres display alterations in proliferation for which hyperactivation of the mechanistic target of rapamycin (mTOR) signaling pathway is the primary cause of neurogenesis deregulation in the absence of CSP-α. In addition, RGL cells lose quiescence upon specific conditional targeting of CSP-α in adult neural stem cells. Our findings demonstrate an unanticipated cell-autonomic and circuit-independent disruption of postnatal neurogenesis in the absence of CSP-α and highlight a direct or indirect CSP-α/mTOR signaling interaction that may underlie molecular mechanisms of brain dysfunction and neurodegeneration.

adult neurogenesis | DNAJC5 | adult-onset neuronal ceroid lipofuscinosis | synaptic neurodegeneration | lysosome

Hippocampal postnatal neurogenesis is a remarkable form of neural plasticity based on the integration of newborn neurons in preexisting neural circuits in the adult brain (1). Multiple studies support the notion that adult neurogenesis is important for learning and memory recall, particularly in the performance of behavioral pattern separation (2–4). Significant progress has been made in recent years in understanding the molecular, cellular, and synaptic mechanisms that regulate and perturb adult neurogenesis (5). In the dentate gyrus, radial glia-like (RGL) stem cells constitute a relatively quiescent cell population that undergoes self-renewal and commits to either an astrocytic or neuronal cell fate (6, 7). The generation of new neurons occurs through sequential differentiation steps of proliferating intermediate neural progenitors that evolve into postmitotic immature neurons before finally becoming mature hippocampal granule cells (5). Critical points of regulation of postnatal neurogenesis are the maintenance of quiescence (8) and neuronal survival (9). The molecular mechanisms underlying these key phenomena, and factors that can perturb them, nevertheless remain poorly understood. Recent studies have emphasized the importance of molecular chaperones to control factors that regulate neural stem cell quiescence (10, 11) and to promote the survival of newborn neurons (12).

Cysteine string protein-α (CSP-α) is a molecular cochaperone that belongs to the heat shock protein-40 (Hsp40) family; it forms a trimeric chaperone complex with heat shock cognate-70 (Hsc70) and small glutamine-rich tetratricopeptide containing protein-A (SGTA) (13). Interestingly, CSP-α is required to maintain the stability of the SNARE protein SNAP25 at synaptic terminals (14–16). SNAP25 cannot maintain its function without a chaperone, which is probably due to the molecular stress induced during cycles of assembly and disassembly of the SNARE complex (15, 17). Remarkably, knockout (KO) mice lacking CSP-α suffer from a devastating and early synaptic degeneration (18) that is particularly evident in highly active neurons (19). The early lethality of CSP-α KO mice has so far impaired the performing of functional in vivo studies of CSP-α in adulthood. Molecular mechanisms of neurodegeneration, although not yet well understood, are linked to damage of SNAP25 (20) when CSP-α is absent. Interestingly, CSP-α is linked to human disease (21). The Parkinson's disease-linked protein, α-synuclein, cooperates with CSP-α to chaperone the SNARE complex (14). Moreover, mutations in the human gene encoding CSP-α (DNAJC5) cause adult-onset neuronal ceroid lipofuscinosis (22).

Although the expression of CSP-α in nonneural tissues was reported long ago (23), little attention has been paid to its functions beyond the synapse. Here, we have found that hippocampal RGL stem cells express CSP-α, which prompted us to

Significance

Neural stem cells generate newborn neurons in the postnatal brain by a process known as neurogenesis. Cysteine string protein-α (CSP-α) maintains healthy nerve terminals and, when mutated in humans, causes a serious disease known as neuronal ceroid lipofuscinosis related to lysosomal pathologies. We have now found that neural stem cells without CSP-α hyperproliferate, leading to depletion of the neural stem cell pool in the mouse hippocampus. Biochemically, the hyperproliferation occurs through the hyperactivation of the mechanistic target of rapamycin (mTOR) signaling pathway. Our findings demonstrate the disruption of postnatal neurogenesis in the absence of CSP-α and unveil an intriguing signaling interaction between CSP-α and mTOR that may underlie molecular mechanisms of brain dysfunction and neurodegeneration.

Author contributions: J.L.N.-G., L.G.-S., F.M., P.L.-C., R.P., and R.F.-C. designed research; J.L.N.-G., L.G.-S., F.M., P.L.-C., M.C.R., and M.V.-V. performed research; J.L.M.-B. contributed new reagents/analytic tools; J.L.N.-G., L.G.-S., F.M., and P.L.-C. analyzed data; and J.L.N.-G. and R.F.-C. wrote the paper.

The authors declare no conflict of interest.

This article is a PNAS Direct Submission.

[1]J.L.N.-G. and L.G.-S. contributed equally to this work.

[2]To whom correspondence may be addressed. Email: jlnieto@us.es or rfchacon@us.es.

This article contains supporting information online at www.pnas.org/lookup/suppl/doi:10.1073/pnas.1817183116/-/DCSupplemental.

Published online March 29, 2019.

investigate the potential role of CSP-α in postnatal neurogenesis. Interestingly, we have found striking alterations in neurogenesis in the dentate gyrus of CSP-α KO mice: RGL escape from the quiescent state, inducing hyperproliferation of intermediate neural progenitors and exhausting the neural stem cell pool. Importantly, this deregulation of neurogenesis is caused by hyperactivation of the mechanistic target of rapamycin (mTOR) pathway and can be rescued in vitro and in vivo upon pharmacological blocking of the kinase activity of mTOR-complex 1 (mTORC1) with rapamycin. The use of conditional KO mice shows that the phenotype also arises upon inducing the genetic removal of CSP-α in RGL cells in adulthood. Our study reveals a key unforeseen implication of a molecular cochaperone whose absence disrupts cell cycle progression in neural stem cells.

Results

Increased Number of Hippocampal Newborn Neurons in CSP-α KO Mice. CSP-α is a synaptic vesicle protein universally expressed in central and peripheral nerve terminals (24); however, its expression and function in nonneuronal cells, such as neural stem cells, have not yet been studied. To precisely identify these cells, we used CSP-α KO mice and control littermates expressing GFP under the nestin promoter (25) (Fig. 1*A*). We examined the hippocampal subgranular zone (SGZ) with antibodies against CSP-α and found that in control mice, beyond the prominent synaptic localization, CSP-α was present in RGL neural stem cells. These cells were easily identified as GFP$^+$ cells exhibiting a characteristic glial fibrillary acidic protein-positive (GFAP$^+$) process extending perpendicularly into the molecular layer of the dentate gyrus (Fig. 1*A*, squares and Movie S1). As expected, we did not detect any CSP-α expression in CSP-α KO mice (*SI Appendix*, Fig. S1). Next, we looked for potential alterations in cell division by monitoring cell cycle activity through the incorporation of the thymidine analog 5-bromo-2′-deoxyuridine (BrdU) at the SGZ (Fig. 1 *B*–*E*). CSP-α KO and littermate control mice received a single i.p. injection of BrdU on postnatal day (P) 10 and were killed on P15 (Fig. 1*C*). The number of BrdU-labeled nuclei in the hippocampus was significantly higher in CSP-α KO mice (Fig. 1*B*) [120.9 ± 3.5 cells per section for WT (n = 3) and 146.4 ± 4.7 cells per section for CSP-α KO (n = 3);

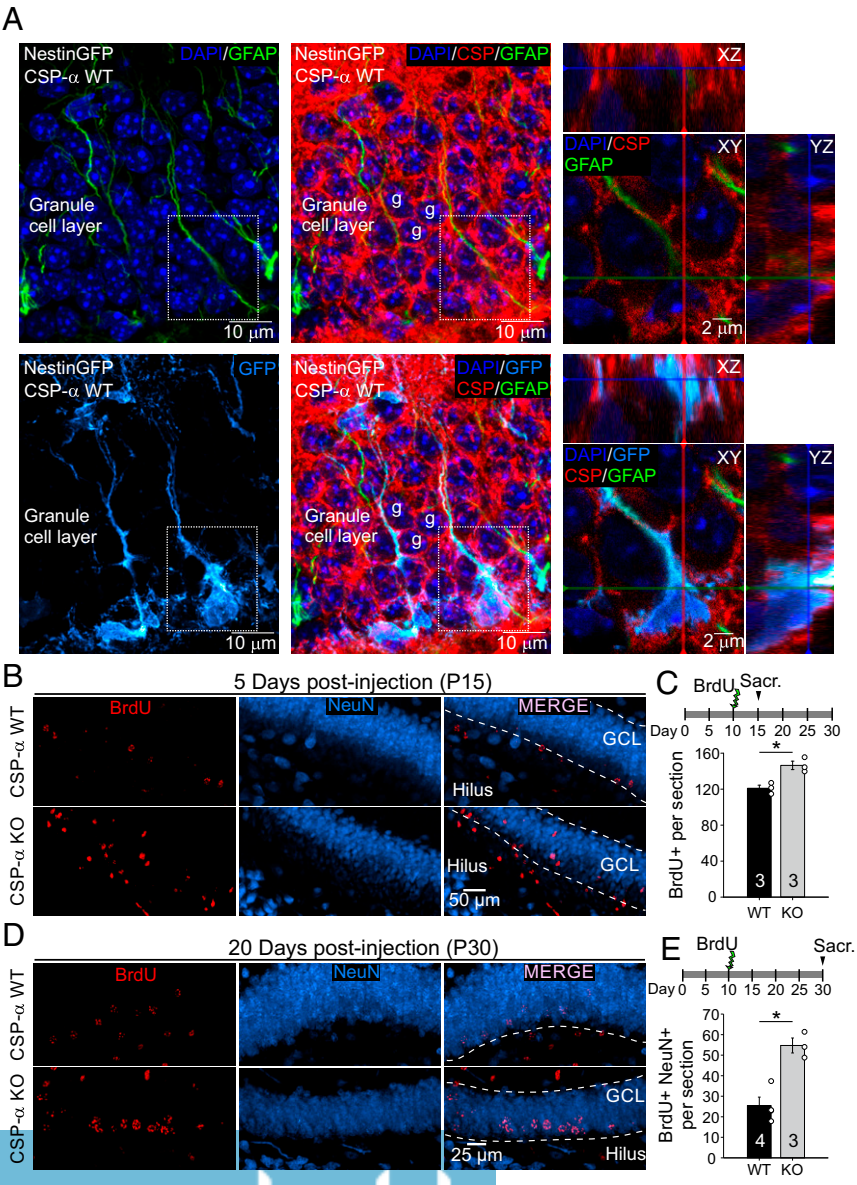

Fig. 1. Postnatal increase of newborn neurons at the hippocampal neurogenic niche in CSP-α KO mice. (*A*, *Left* and *Center*) Maximum intensity projections of a z-stack of confocal images from nestin-GFP transgenic CSP-α WT mouse hippocampal slices labeled with DAPI (dark blue), anti-GFP (light blue), and anti-GFAP (green) antibodies. (*A*, *Right*) Areas within dashed-line squares are magnified, showing three optical sections [XY (*Middle*), XZ (*Upper*), and YZ (*Right*)] of RGLs in the dentate gyrus identified by the colocalization of nestin (blue) and GFAP (green). Better visualization is provided in Movie S1. We have found that 100% of nestin$^+$/GFAP$^+$ cells express CSP-α (28 cells observed in three different mice). (*B*) Maximum intensity projection of a z-stack of confocal images of CSP-α WT and KO hippocampal slices labeled with antibodies against BrdU (red) and NeuN (blue) 5 d after BrdU injection. (*C*) Increased number of BrdU$^+$ nuclei per section in CSP-α KO mice compared with WT mice 5 d postinjection (four sections per mouse for WT and four to five sections per mouse for CSP-α KO; n = 3 for each genotype). Sacr., sacrifice. (*D*) Maximum intensity projection of a z-stack of confocal images of CSP-α WT and KO hippocampal slices labeled with antibodies against BrdU (red) and NeuN (blue) 20 d after BrdU injection. (*E*) Increased number of newborn neurons identified as BrdU$^+$ nuclei per section colocalizing with NeuN in CSP-α KO mice at 20 d postinjection [four sections per mouse for WT (n = 4) and four and five sections per mouse for CSP-α KO (n = 3)]. Numbers in bars indicate the number of mice used. Mean ± SEM (*P < 0.05, Student's t test).

$P < 0.05$, Student's t test; Fig. 1*C*], which is consistent with higher cell proliferation. To investigate if those cells were newborn neurons, we carried out a second set of experiments wherein mice were again injected with BrdU on P10 but BrdU incorporation was analyzed on P30. Remarkably, the number of newborn neurons, identified as $NeuN^+$ cells with $BrdU^+$ nuclei (Fig. 1*D*), turned out to be twofold higher in CSP-α KO mice compared with controls [25.4 ± 11.3 cells per section for WT ($n = 4$) and 54.7 ± 5.8 cells per section for CSP-α KO ($n = 3$); $P < 0.05$, Student's t test; Fig. 1*E*]. This phenotype could be due to either a net increase in proliferation or, alternatively, a better survival rate under otherwise normal cell proliferation. To distinguish between those two possibilities, we investigated BrdU incorporation during an extremely short postinjection period (2 h; *SI Appendix*, Fig. S2 *A* and *B*). This experiment revealed that the number of cells incorporating BrdU was also higher in CSP-α KO mice (*SI Appendix*, Fig. S2*B*), supporting the notion that in the absence of CSP-α, the higher number of newborn cells is, at least in part, explained by cell hyperproliferation. This finding was further confirmed by a substantial increase in the level of labeling with the mitotic marker Ki-67 (*SI Appendix*, Fig. S2 *C* and *D*). Overall, our data show a clear enhancement in the production of newborn neurons in the hippocampus of CSP-α KO mice that could be explained by cell hyperproliferation. Since our observations demonstrate the expression of CSP-α in RGL neural stem cells, we decided to investigate these cells, the cell lineage immediately derived from them, and their involvement in neuronal differentiation during postnatal neurogenesis.

Fast and Progressive Depletion of the RGL Neural Stem Cell Pool in the CSP-α KO Hippocampal SGZ. We used antibodies against nestin, Sox2, and minichromosome maintenance type 2 (MCM2) to identify all RGL neural stem cells as $nestin^+$, $Sox2^+$ cells and dividing RGL neural stem cells as $nestin^+$, $Sox2^+$, $MCM2^+$ cells in hippocampal slices. On P15, RGL neural stem cells were readily identified in control and CSP-α KO mice as $nestin^+$, $Sox2^+$ cells exhibiting characteristic $nestin^+$ vertical processes (Fig. 2 *A* and *B* and *SI Appendix*, Fig. S3). The number of these cells constituting the neural stem cell pool was similar in WT and CSP-α KO mice (Fig. 2*C*). In contrast, the number of dividing neural stem cells was found to be significantly higher in CSP-α KO mice compared with controls (Fig. 2*C*). Moreover, a most interesting observation was that the proportion of proliferating cells with respect to the total number of RGL cells was increased in the absence of CSP-α. These results suggested that the absence of CSP-α activates cell cycling in neural stem cells. Strikingly, the same analysis carried out at P30 (Fig. 2 *D* and *E*) highlighted a significant reduction in the pool size of $nestin^+$, $Sox2^+$ cells in CSP-α KO mice (886.4 ± 31.1 cells per section for WT and 599 ± 36.5 cells per section for CSP-α KO; $n = 3$ for each genotype; $P < 0.01$, Student's t test; Fig. 2*F*). Interestingly, however, the percentage of proliferating cells ($nestin^+$, $Sox2^+$, $MCM2^+$) relative to the total number of RGL cells (Fig. 2*F*) remained elevated (137 ± 21.2 cells per square millimeter for WT and 234.3 ± 22.9 cells per square millimeter for CSP-α KO; $n = 3$ for each genotype; $P < 0.05$, Student's t test). In addition, we investigated whether the lack of CSP-α in $nestin^+$, $GFAP^+$ or $Sox2^+$, $MCM2^+$ cells from WT mice could be a molecular feature of either transition to proliferation or a proliferative state. This was not found to be the case (Fig. 1*A* and *SI Appendix*, Fig. S4). Overall, those observations reflect that CSP-α may favor a quiescent state and that its absence disinhibits RGL neural stem cell proliferation. In the absence of CSP-α, the unleashing of proliferation progressively leads to an important increase in the proportion of proliferating versus quiescent cells that likely exhausts the stem cell pool. This observation would be consistent with the notion of the limited self-renewal capacity of neural stem cells. To further investigate the developmental progress of newborn cells, we subsequently examined the characteristics of neural intermediate progenitor cells.

Increased Proliferation and Altered Positioning of Neural Intermediate Progenitor Cells. Antibodies against doublecortin (DCX) were used to label neural intermediate progenitor cells (*SI Appendix*, Fig. S5 *A*, light blue, and *B*, blue). In addition, we used antibodies against MCM2 to label dividing neural intermediate progenitor cells (*SI Appendix*, Fig. S5 *A* and *B*, red). Interestingly, the number of DCX^+ cells was found to be much higher in the absence of CSP-α (2,127.2 ± 252.2 cells per square millimeter for WT vs. 4,168.3 ± 239.8 cells per square millimeter for CSP-α KO; $n = 3$ for each genotype; $P < 0.05$, Student's t test; *SI Appendix*, Fig. S5*C*). MCM2 nuclear labeling, in contrast, allows the quantification of dividing neural intermediate progenitor cells (DCX^+, $MCM2^+$). The number of DCX^+, $MCM2^+$ cells was elevated in the dentate gyrus of CSP-α KO mice, whereas the percentage of actively dividing DCX^+ cells (DCX^+, $MCM2^+$/total $MCM2^+$ ratio; *SI Appendix*, Fig. S5*C*) was the same as that in the WT controls (43 ± 2% for WT and 45 ± 5% for CSP-α KO; $n = 3$ for each genotype; $P > 0.05$, Student's t test). These observations suggested that the increased mitotic activity of RGL stem cells ($nestin^+$, $Sox2^+$ cells) translated into a high number of DCX^+ cells, following the expected progression of cell differentiation steps, once postnatal neurogenesis has been activated. Curiously, a close examination of $MCM2^+$ cells (Fig. 2*B*) in the dentate gyrus of CSP-α KO mice revealed a widespread distribution of those cells across the entire granule cell layer in contrast to the confined positioning of the same cell type characteristically observed in the SGZ of WT mice (*SI Appendix*, Fig. S5*D*). Taken together, these findings highlight a clear dysfunction of neurogenesis in the absence of CSP-α caused by an as yet unknown mechanism. Hippocampal neurogenesis is regulated by GABAergic synaptic inputs from parvalbumin-expressing interneurons (8, 26). As such, the observed alterations in neurogenesis could perhaps be explained by a secondary effect of GABAergic synaptic degeneration as previously described for CSP-α KO mice (19).

Normal GABA Spontaneous Release onto Dentate Gyrus Granule Cells. To investigate if any GABAergic synaptic degeneration in CSP-α KO mice occurs earlier than 3 wk as previously described (19), we recorded miniature inhibitory postsynaptic currents produced by granule cells in response to the spontaneous release of GABA released from parvalbumin-positive cells (*SI Appendix*, Fig. S6 *A* and *B*). We could not identify significant differences in the amplitude, kinetics, or frequency of events in mutant and control mice (*SI Appendix*, Fig. S6 *C–F*). These observations are consistent with the notion that no neurodegenerative changes to GABAergic synaptic inputs take place at early postnatal ages in the CSP-α KO dentate gyrus. Based on these findings, we ruled out the possibility that the loss of quiescence was due to alterations in the GABAergic neuronal circuitry. Consequently, we decided to study circuit-independent mechanisms that could explain our findings.

Hyperproliferation of Cultured Neurospheres Obtained from the CSP-α KO Mouse Hippocampus. We cultured neurospheres from hippocampi of newborn mice to obtain suitable conditions to study circuit-independent mechanisms of neural stem cell proliferation in vitro. Our neurospheres were healthy and enriched in neural stem cells, and expressed CSP-α (*SI Appendix*, *SI Results* and Figs. S7 and S8). Although CSP-α KO neurospheres grew well in culture, they were noticeably larger than neurospheres prepared from WT mice (*SI Appendix*, Fig. S9 *A–C*). A possible explanation for this difference could be due to an augmented cellularity in the event that mitotic activity was intrinsically increased. To investigate this possibility, we dissociated the neurospheres, labeled the cells with fluorescently labeled antibodies against the proliferation marker antigen Ki-67, and quantified the number

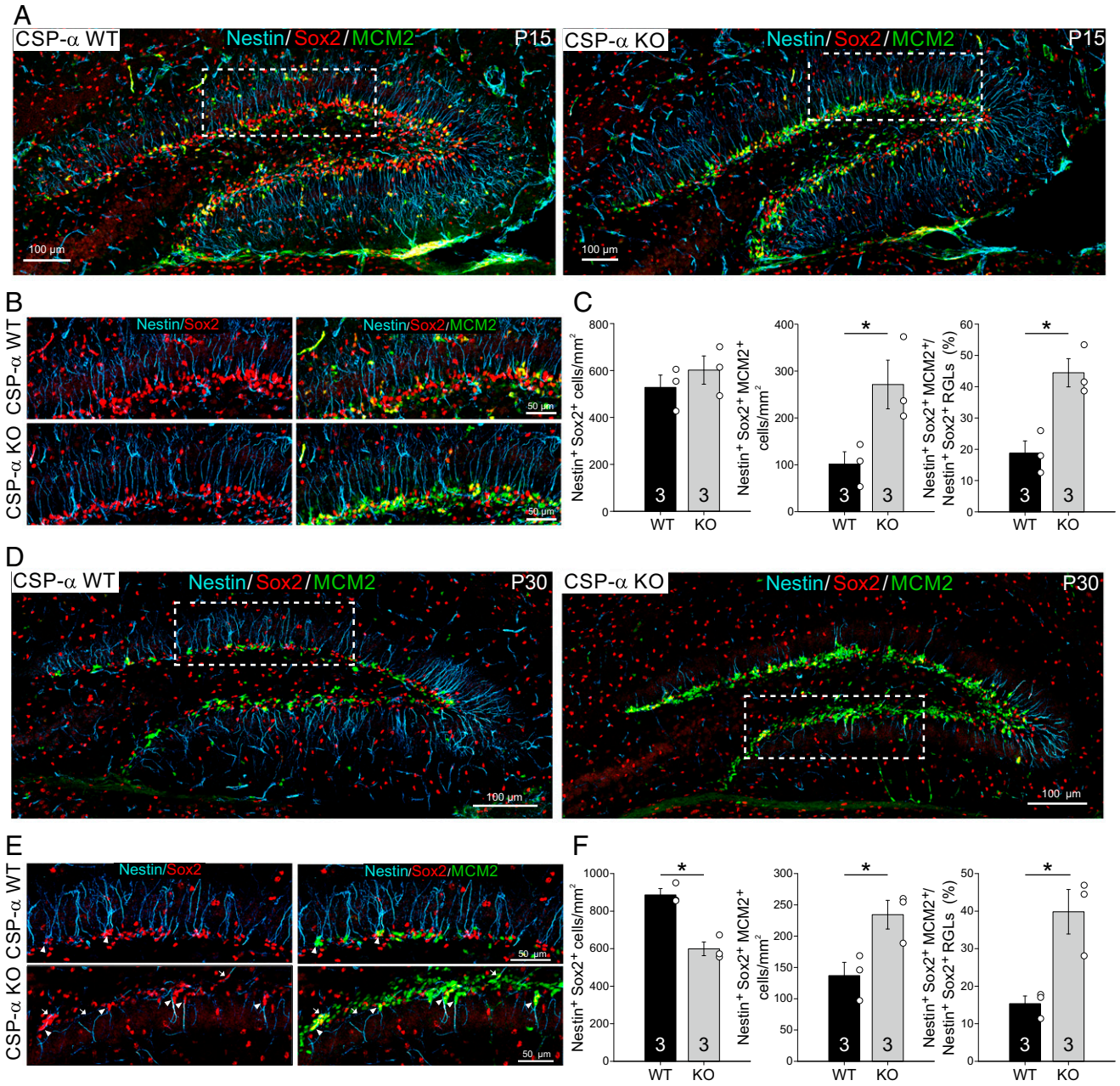

Fig. 2. Quiescence loss and RGL pool depletion in the dentate gyrus of CSP-α KO mice. (*A*) Maximum intensity projection of a z-stack of confocal images of CSP-α WT and KO hippocampal dentate gyri labeled with antibodies against nestin (blue), Sox2 (red), and MCM2 (green) at P15. (*B*) Magnification of the area enclosed within the dashed-line squares in *A*. (*C*) At P15, no significant differences are apparent in the size of the RGL cell pool (nestin$^+$, Sox$^+$ cells per square millimeter), but the number (nestin$^+$, Sox$^+$, MCM2$^+$ cells per square millimeter) and percentage of dividing RGL cells are strongly increased in CSP-α KO mice compared with WT controls (five to six sections per mouse for WT and five to six sections per mouse for CSP-α KO; $n = 3$ for each genotype). (*D*) Maximum intensity projection of a z-stack of confocal images of CSP-α WT and KO hippocampal dentate gyri labeled with antibodies against nestin (blue), Sox2 (red), and MCM2 (green) at P30. (*E*) Magnification of the area enclosed within the dashed-line squares in *D*. (*F*) At P30, the RGL cell pool size (nestin$^+$, Sox$^+$ cells per square millimeter) is clearly reduced and the number (nestin$^+$, Sox$^+$, MCM2$^+$ cells per square millimeter) and percentage of dividing RGL cells are strongly increased in CSP-α KO mice compared with WT controls (six to seven sections per mouse for WT and seven sections per mouse for CSP-α KO; $n = 3$ for each genotype). Numbers in bars indicate the number of mice used. Mean ± SEM (*$P < 0.05$, Student's *t* test).

of dividing cells. Consistent with the notion of a higher mitotic activity, the number of Ki-67$^+$ cells was significantly increased in CSP-α KO neurospheres (*SI Appendix*, Fig. S9*D*). We also carefully monitored the number of neurospheres over time in culture and quantified them at every passage. The time course of the number of neurospheres, examined along seven consecutive passages, was found to be different in the mutant mice compared with WT controls. We plotted the percentage of the number of neurospheres produced per passage normalized to littermate WT controls (*SI Appendix*, Fig. S9*E*, *Right*) and aligned those plots to the maximum peak of every culture versus the relative passage number (*SI Appendix*, Fig. S9*E*, *Left*) to study the average growing trend of all the mutant cultures. The amplitude of the peak (at relative passage 0) was significantly different from the amplitude at relative passage number −3 ($P = 0.0286$, Mann–Whitney *U* test), but not from the amplitude at relative passage number +2 when proliferation

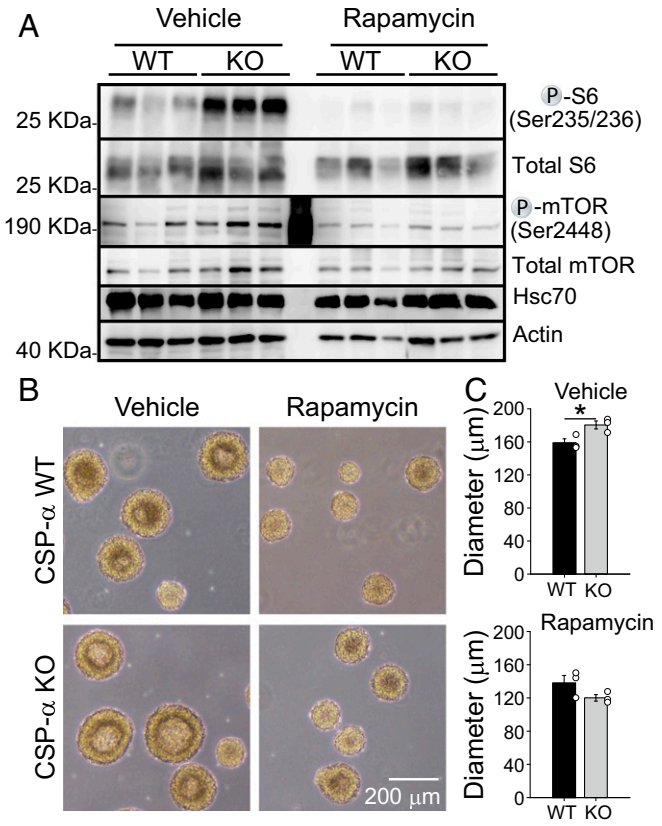

Fig. 3. Hyperactivation of the mTORC1 signaling pathway causes hyperproliferation in CSP-α KO neurospheres. (*A*) Rapamycin (25 nM) strongly inhibited the phosphorylation of ribosomal protein S6 in WT and CSP-α KO neurosphere cultures ($n = 3$ cultures from three mice for each genotype). (*B*) Typical images of WT and CSP-α KO cultures incubated in vehicle or rapamycin (25 nM) for 7 d starting from the time at which cells were cultured. (*C*) Incubation in the presence of rapamycin (25 nM), compared with incubation in vehicle, reestablished the normal neurosphere size in CSP-α KO cultures (mean value of $P < 0.05$, Student's *t* test). Rapamycin decreased the size of both WT and CSP-α KO neurospheres.

decreased in the mutant-type neurospheres ($P = 0.0576$, Mann–Whitney *U* test). Although these results suggest that hypoproliferation occurs after hyperproliferation, only the existence of the hyperproliferation ascending phase was statistically significant. Such a finding, however, could suggest an initial deregulated increase in neurosphere-forming efficiency, reflecting an increase in stem cell proliferation leading to stem cell depletion, similar to what happened in situ to the hippocampal stem cell pool (Fig. 2). These observations suggest that the absence of CSP-α disrupts stem cell quiescence by a circuit-independent mechanism. While such a role for CSP-α was unexpected, the relative cellular homogeneity of neurospheres compared with the brain nevertheless provides advantages to search for possible molecular mechanisms underlying this effect.

Hyperactivation of the mTOR Signaling Pathway Causes Hyperproliferation of Neurospheres. The role of CSP-α as a cochaperone involved in maintaining the stability of the SNARE complex, particularly the SNARE protein SNAP25, is well established (14, 15). We examined levels of the SNARE proteins SNAP23, SNAP25, and SNAP29 in neurospheres and found that SNAP25 is practically absent, while the levels of the more abundant SNAP23 and SNAP29 were similar in CSP-α KO and WT neurospheres (*SI Appendix*, Fig. S10). Next, we searched for proteins related to CSP-α [CHL1 (27) and dynamins (28)] and explored proteins and pathways involved in neural stem cell proliferation [p27 (11, 29), Wnt/β-catenin (30), Notch (31), sonic hedgehog (Shh) (32), and PI3K/Akt/mTOR (33)]. We only found changes in the mTOR signaling pathway, revealed by increased levels of the phosphorylated form of the ribosomal protein S6 (pS6) (Fig. S10), which is indicative of the activation of the kinase S6K, a downstream target of the mTORC1 pathway. This suggested that, in cultured neurospheres, CSP-α might directly or indirectly act as a down-regulator of the mTORC1-dependent signaling pathway. It is well established that mTORC1 hyperactivation stimulates cell cycle progression through the downstream effector S6K1 and the translational inhibitor 4E-BP in a rapamycin-sensitive manner (34). Accordingly, we decided to test the rapamycin effect on neurospheres in culture from mutant and control mice. We incubated neurospheres in rapamycin (25 nM) for 7 d, starting from the time at which cells were cultured, and identified robust inhibition of S6 phosphorylation, which was detected in both genotypes but was particularly evident in protein extracts from mutant cells that, under control conditions, confirmed prominent levels of S6 phosphorylation compared with WT samples (Fig. 3*A*). Interestingly, as previously observed (*SI Appendix*, Fig. S9), the size of CSP-α KO neurospheres incubated in vehicle was larger than that of WT neurospheres grown under the same conditions (Fig. 3 *B* and *C*). In contrast, upon treatment with rapamycin, the size of the mutant neurospheres became similar to that of WT neurospheres (Fig. 3 *B* and *C* and *SI Appendix*, Fig. S11), consistent with the notion that overgrowth in the absence of CSP-α is produced by the hyperactivation of mTORC1-dependent signaling. These results suggest that the hyperproliferation of RGL stem cells seen in the hippocampus (Fig. 2) could be due to the hyperactivation of mTOR-dependent mechanisms that control cell cycle progression. To check this, we decided to determine if the rapamycin-mediated rescue of proliferation in neurospheres in vitro could be translated to in vivo conditions.

Rapamycin-Mediated Blocking of the mTOR Signaling Pathway Rescues Neurogenesis Dysfunction in CSP-α KO Mice in Vivo. We administered vehicle or rapamycin to mice (10 mg/kg) starting at P10 and continuing through P30, whereupon animals were killed for analysis (Fig. 4*A*). As previously observed (Fig. 2), in the group of mice treated with vehicle only, the number of dividing cells identified as $MCM2^+$ cells (Fig. 4*B*) increased dramatically in the CSP-α KO hippocampus compared with WT controls (1,204.4 ± 23.5 cells per square millimeter for WT in vehicle and 2,660 ± 201.9 cells per square millimeter for CSP-α KO in vehicle; $n = 3$ for each genotype; $P < 0.05$, two-way ANOVA; Fig. 4*D*, *Left*). Remarkably, the number of dividing RGL cells ($nestin^+$, $Sox2^+$, $MCM2^+$ cells) was also increased in CSP-α KO mice (124 ± 4 cells per square millimeter for WT in vehicle and 194 ± 4.9 cells per square millimeter for CSP-α in vehicle; $n = 3$ for each genotype; $P < 0.05$, two-way ANOVA). In addition, for the same conditions, the total number of RGL stem cells ($nestin^+$, $Sox2^+$ cells) was found to be significantly lower in the mutants [506 ± 7.7 cells per square millimeter for WT ($n = 4$) and 308 ± 26.3 cells per square millimeter for CSP-α KO ($n = 5$); $P < 0.05$, two-way ANOVA; Fig. 4*D*], and the percentage of dividing RGL stem cells ($nestin^+$, $Sox2^+$, $MCM2^+$ cells normalized to the total number of RGL cells) was clearly increased in the absence of CSP-α (25 ± 1.3% for WT in vehicle and 55 ± 3.5% for CSP-α KO in vehicle; $n = 3$ for each genotype; $P < 0.05$, two-way ANOVA; Fig. 4*D*, *Right*). We then analyzed the changes induced by rapamycin. Remarkably, treatment with rapamycin did not induce changes in any of the parameters in WT mice compared with vehicle. In contrast, rapamycin dissipated the differences between RGL cells from CSP-α KO and WT mice (Fig. 4 *C* and *D*). In the CSP-α KO mice, rapamycin reduced the number of dividing cells ($MCM2^+$ cells) (2,660 ± 201.9 cells per square millimeter for CSP-α KO in vehicle vs. 1,735 ± 202.8 cells per square millimeter for CSP-α KO in rapamycin; $n = 3$ for each condition; $P < 0.05$, two-way ANOVA; Fig. 4*D*, *Left*) and the

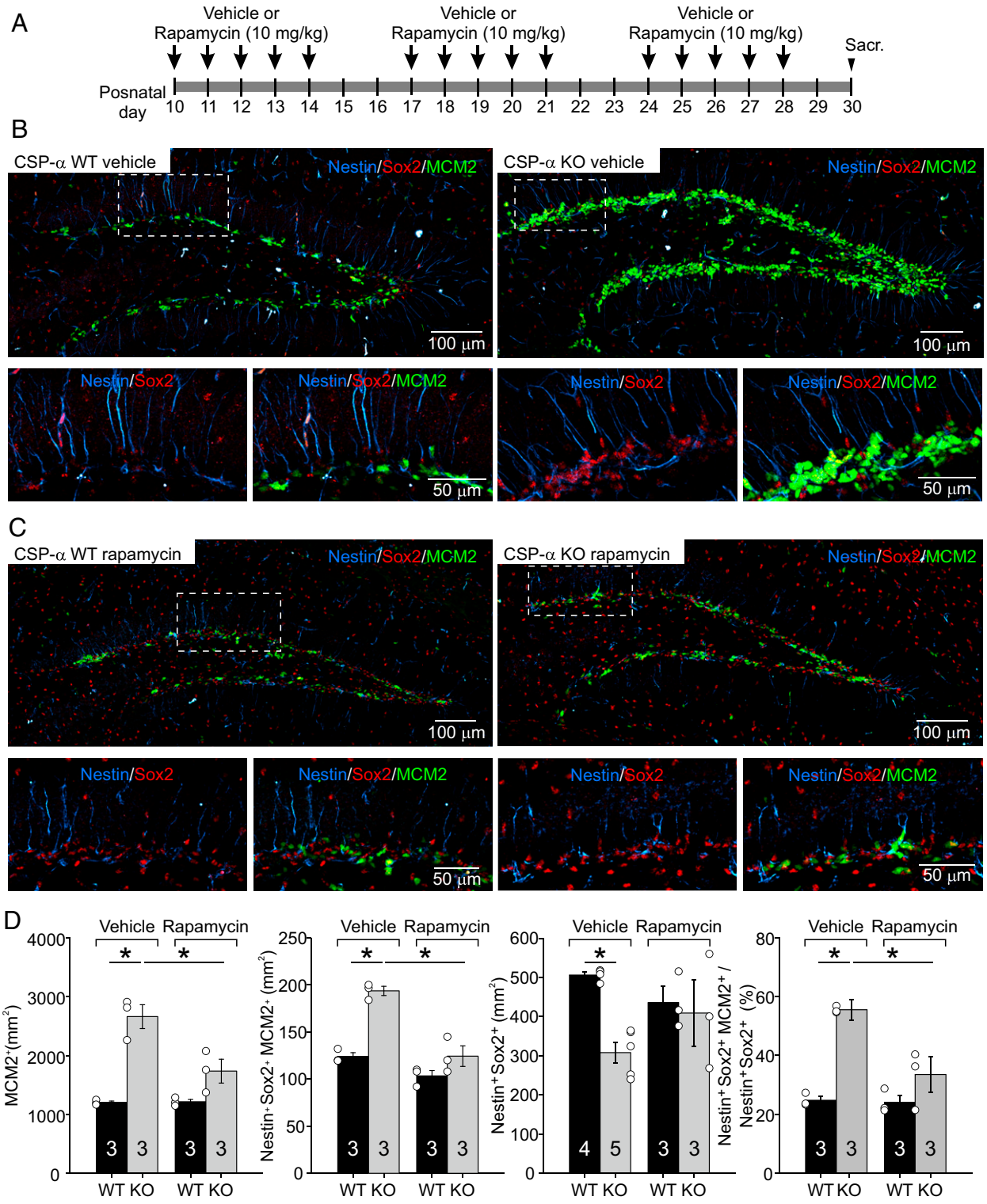

Fig. 4. Rescue of neural stem cell quiescence in vivo upon pharmacological inhibition of the mTORC1-dependent signaling pathway in CSP-α KO mice. (*A*) Time line for treatment with vehicle or rapamycin (10 mg/kg). Sacr., sacrifice. (*B*) Maximum intensity projection of a z-stack of confocal images of CSP-α WT and KO hippocampal dentate gyri labeled with antibodies against nestin (blue), Sox2 (red), and MCM2 (green) from 30-d-old mice treated with vehicle. Magnified views (*Lower*) of the areas in dashed squares (*Upper*) show the notable increase in neurogenic proliferation ($MCM2^+$ cells in green, arrowheads) in CSP-α KO mice. (*C*) Confocal images, as in A, taken from 30-d-old mice treated with rapamycin (10 mg/kg, administered once per day for 5 consecutive days per week for ∼20 d). Magnified views (*Lower*) of areas in dashed squares (*Upper*) show the strong reduction in the number of $MCM2^+$ cells (green, arrowheads) in CSP-α KO mice, indicating the normalization of stem cell proliferation upon pharmacological inhibition of the mTORC1-dependent signaling pathway. (*D*) Rapamycin reestablishes the total number of proliferating cells ($MCM2^+$ cells; *Left*), the number of dividing RGL stem cells ($nestin^+$, $Sox2^+$, $MCM2^+$ cells; *Center*), and the percentage of activated proliferating RGL stem cells (*Right*) (four to six sections per mouse for WT and KO; $n = 3$ for each genotype, except for quantification of $nestin^+$, $Sox2^+$ cells of mice treated with vehicle) to WT levels. Numbers in bars indicate the number of mice used. Values represent mean ± SEM (*$P < 0.05$, two-way ANOVA).

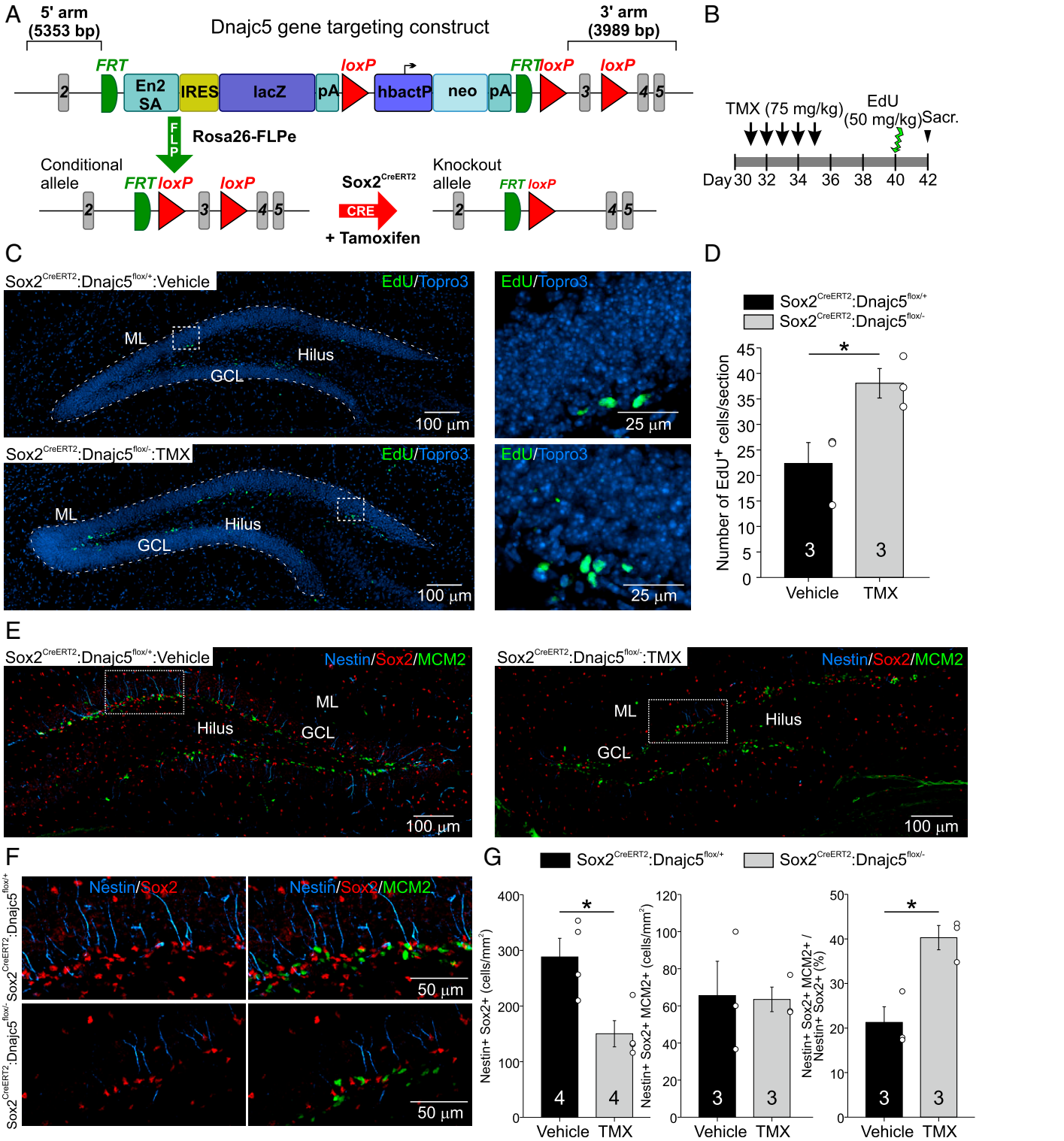

Fig. 5. Increased proliferation and loss of quiescence in RGLs lacking CSP-α in the dentate gyrus of the *Sox2*^{CreERT2}:*Dnajc5*$^{flox/-}$ conditional mouse model. (*A*) Genomic strategy for cre-recombinase-dependent deletion at Dnajc5 mouse locus. (*B*) Timeline for treatment with tamoxifen (TMX; 75 mg/kg) and EdU (50 mg/kg). (*C*) Maximum intensity projection of a z-stack of confocal images of slices labeled with EdU and TO-PRO-3. Slices were obtained from *Sox2*^{CreERT2}:*Dnajc5*$^{flox/+}$ animals injected with vehicle and *Sox2*^{CreERT2}:*Dnajc5*$^{flox/-}$ animals injected with TMX (75 mg/kg). (*D*) Increased number of EdU-positive nuclei per section in *Sox2*^{CreERT2}:*Dnajc5*$^{flox/+}$:vehicle compared with *Sox2*^{CreERT2}:*Dnajc5*$^{flox/-}$:TMX animals at 2 d postinjection (dpi) of EdU (6–7 sections/mouse, $n = 3$ for each genotype). (*E*) Maximum intensity projections of a z-stack of confocal images of *Sox2*^{CreERT2}:*Dnajc5*$^{flox/+}$:vehicle and *Sox2*^{CreERT2}:*Dnajc5*$^{flox/-}$:TMX hippocampal dentate gyri labeled with antibodies against nestin (blue), Sox2 (red), and MCM2 (green) are shown at P42. (*F*) Magnification of the area enclosed within the dashed-line square in *C*. (*G*) Size of the RGL cell pool (nestin$^+$, Sox2$^+$ cells per square millimeter; six to seven sections per mouse; $n = 4$ for each genotype) is significantly decreased, and the percentage of dividing RGL cells (six to seven sections per mouse; $n = 3$ for each genotype) is significantly increased in *Sox2*^{CreERT2}:*Dnajc5*$^{flox/-}$:vehicle mice compared with *Sox2*^{CreERT2}:*Dnajc5*$^{flox/-}$:TMX mice. No differences were found in the number of dividing RGL cells (nestin$^+$, Sox2$^+$, MCM2$^+$ cells per square millimeter; six to seven sections per mouse; $n = 3$ for each genotype). Quantifications after tamoxifen treatment for 12 d. $^*P < 0.05$. White circles correspond to values from individual mice.

number of proliferating RGL cells (nestin$^+$, Sox2$^+$, MCM2$^+$ cells) (194 ± 4.9 cells per square millimeter for CSP-α KO in vehicle vs. 124 ± 10.9 cells per square millimeter for CSP-α KO in rapamycin; $n = 3$ for each condition; $P < 0.05$, two-way ANOVA). Importantly, although we could not detect significant changes in the total numbers of RGL cells (nestin$^+$, Sox2$^+$ cells) in CSP-α KO mice under both conditions (Fig. 4*D*), rapamycin decreased the proportion of dividing RGL cells (nestin$^+$, Sox2$^+$, MCM2$^+$ cells) in the CSP-α KO (55 ± 3.5% for CSP-α KO in vehicle vs. 33 ± 6.0% for CSP-α KO in rapamycin; $n = 3$ for each condition; $P < 0.05$, two-way ANOVA; Fig. 4*D*, *Right*).

Overall, our observations indicate that the uninhibited hyperproliferation of RGL cells that leads to a progressive, fast, and severe depletion of the stem cell pool is fully reversible upon pharmacological treatment with rapamycin. Furthermore, these results indicate that the absence of CSP-α in vivo disrupts neural stem cell quiescence, allowing uncontrolled cell cycle progression downstream of the mTORC1 signaling pathway. As CSP-α is expressed in virtually every neuron, it is difficult to conclude from the observations in a conventional KO mouse model that the loss of quiescence in vivo unequivocally constitutes a cell-autonomous mechanism rather than being secondary to an unknown neuronal alteration. To solve this caveat, we proceeded to generate a conditional CSP-α KO mouse to specifically remove CSP-α from RGLs in a time-controlled manner.

Loss of Quiescence in Adult RGLs in Vivo by Conditional Specific Targeting of CSP-α in Neural Stem Cells. We used mouse embryonic stem (ES) cells harboring a modified allele of *Dnajc5* (the mouse gene coding for CSP-α) with loxP sites flanking exon 2 (Fig. 5*A*) to generate a mouse line for the conditional deletion of CSP-α (*Experimental Procedures*). Once the mice were generated, we bred them against the *UBC*^{CreERT2} line in which Cre-recombinase activity is induced under the promoter of the ubiquitin C human gene in widespread cells and tissues and only in the presence of tamoxifen. The neurological phenotype, early lethality, and analysis of protein levels in these mice validated the genomic strategy to generate further conditional CSP-α KO mouse lines (*SI Appendix*, *SI Results* and Fig. S12). Next, to investigate the consequences of removing CSP-α from neural stem cells, we used Sox2^{CreERT2} transgenic mice, which have been previously used specifically to induce Cre-recombinase activity with tamoxifen in hippocampal neural stem cells (35). We bred this line with the *Dnajc5*$^{flox/flox}$ and CSP-α heterozygous mice to obtain *Sox2*^{CreERT2}:*Dnajc5*$^{flox/+}$ and *Sox2*^{CreERT2}:*Dnajc5*$^{flox/-}$ littermate mice to be used for experiments. The rationale behind this strategy was to halve the floxed allele genetic load to maximize the Cre-recombinase efficiency in *Sox2*^{CreERT2}:*Dnajc5*$^{flox/-}$ mice. Tamoxifen has been widely used as a tool to investigate neurogenesis in conditional KO mouse lines, and the lack of effect of this molecule on neural stem cells is well documented (36). In addition, we independently showed that tamoxifen itself does not have any effect on cell proliferation at the hippocampal SGZ in WT mice (*SI Appendix*, Fig. S13). We set two experimental groups in our study: *Sox2*^{CreERT2}:*Dnajc5*$^{flox/+}$ mice injected with vehicle as control mice and *Sox2*^{CreERT2}:*Dnajc5*$^{flox/-}$ mice injected with tamoxifen to investigate neural stem cell biology in the absence of CSP-α (Fig. 5*B*). We analyzed the number of cell nuclei labeled with 5-ethynyl-2′-deoxyuridine (EdU) in hippocampal slices at the SGZ and found a significant increase of EdU$^+$ cells in *Sox2*^{CreERT2}:*Dnajc5*$^{flox/-}$ mice compared with controls (22.3 ± 4.1 cells per section for WT and 38.1 ± 2.9 cells per section for CSP-α KO; $n = 3$ for each genotype; $P < 0.05$; Fig. 5 *C* and *D*), indicating higher proliferation activity as a consequence of CSP-α targeting. Next, we used immunohistochemistry to specifically explore RGL cells and found that the total number of RGL cells (nestin$^+$, Sox2$^+$), but not dividing RGL cells (nestin$^+$, Sox2$^+$, MCM2$^+$), was significantly decreased in the *Sox2*^{CreERT2}:*Dnajc5*$^{flox/-}$ mice compared with control mice [*Sox2*^{CreERT2}:*Dnajc5*$^{flox/+}$ in vehicle: 288.3 ± 33.4 cells per square millimeter ($n = 4$), *Sox2*^{CreERT2}:*Dnajc5*$^{flox/-}$ in tamoxifen: 150.2 ± 23.6 cells per square millimeter ($n = 4$); $P < 0.05$; Fig. 5 *E*–*G*]. The percentage of dividing RGL stem cells was clearly increased in *Sox2*^{CreERT2}:*Dnajc5*$^{flox/-}$ mice (Fig. 5*G*). Taken together, these observations are consistent with the results obtained with CSP-α KO mice in vivo and in cultured neurospheres, and support the notion that CSP-α plays a key role in maintaining the quiescence of hippocampal neural stem cells by a mechanism independent of neuronal circuitry, and not secondary to any paracrine input associated with neuronal alterations.

Discussion

Our study has identified the cochaperone CSP-α as a key factor that either directly or indirectly impacts the maintenance of neural stem cell quiescence in the postnatal dentate gyrus. Such a role is surprising because the major established functions for CSP-α as a cochaperone have been mainly restricted to the synaptic terminals so far (14–16, 18–21). We have demonstrated that CSP-α is present in situ in RGL neural stem cells in the dentate gyrus (Fig. 1) and in cultured neurospheres (*SI Appendix*, Fig. S7). Consistent with our observations, the expression of CSP-α in quiescent neural stem cells has been reported in several recent single-cell transcriptomic analyses of the adult SGZ and subventricular zone (37–39) and in a proteomic study carried out on human neural stem cells derived in vitro from ES cells (40). We have clearly shown that the proliferation of hippocampal RGL cells is dramatically increased in CSP-α KO mice (Fig. 2). At P15, the total number of RGL cells was the same in mutant and control mice (Fig. 2). In contrast, at P30, the total number of RGL cells was strongly reduced compared with control mice (Fig. 2), suggesting that maintained hyperproliferation causes progressive exhaustion of the stem cell pool. Such a phenotype could be consistent with a disruption of asymmetrical self-renewal, and, although beyond the scope of this study, it is potentially of significant interest to study the mechanisms and capacities for long-term self-renewal of neural stem cells (6, 7). Since CSP-α KO mice die early (around 4–5 wk of age), we generated inducible conditional mice in which CSP-α is eliminated specifically in neural stem cells after 1 mo of age (Fig. 3) to investigate how important CSP-α is for adult neurogenesis. Interestingly, in these mice, similar to what we observed in the dentate gyrus of conventional CSP-α KO mice, neural stem cells displayed a clearly hyperproliferative phenotype (Fig. 3). These observations also support the notion that CSP-α plays a direct or indirect role, but not secondary to neurodegeneration, in the maintenance of neural stem cell quiescence. Most likely that role is cell-autonomous; however, we cannot completely rule out that CSP-α KO in intermediate progenitors might feed back to neural stem cells to proliferate in a paracrine manner.

Our data show that the downstream target of mTORC1, SK6 kinase, increases its kinase activity in the absence of CSP-α, which is likely triggered by hyperactivation of the mTORC1 (Fig. 4 and *SI Appendix*, Fig. S10). Consistent with this notion, rapamycin suppressed the S6 hyperphosphorylation (Fig. 4) and reverted the characteristic hyperproliferative phenotype observed in CSP-α KO mice, in vitro in cultured neurospheres (Fig. 4 and *SI Appendix*, Fig. S11) and in vivo in the dentate gyrus, to WT levels (Fig. 5). How and which other proteins within the full mTOR pathway become modified upon removal of CSP-α is an open issue that requires deeper investigations. The pivotal role of mTORC1 in controlling the self-renewal, proliferation, and differentiation of several types of stem cells (41, 42), including adult neural stem cells (43, 44), is well established. Consistent with our observations (Figs. 2, 3, and 5), evidence in the literature indicates that persistent mTORC activation in different types of nonneural stem cells increases cell proliferation and ultimately induces stem cell exhaustion (45, 46). Indeed, mTORC1 hyperactivation is a biochemical hallmark of

the tuberous sclerosis complex (TSC), a multisystem genetic disorder caused by loss of function of the TSC1/TSC2 heterodimer that physiologically regulates mTORC1 activation. Notably, there are certain similarities between the neural stem cell phenotypes present in CSP-α KO mice and the phenotypes found in TSC mouse models (41) and other mouse models (43), with mutations that lead to mTOR hyperactivation. Notably, Hsc70 interacts with TSC2, and, furthermore, the interaction is stronger with the pathogenic TSC2 R611Q version (47). This mutant version does not interact with TSC1 and fails to inhibit S6K-T389 phosphorylation (48) likely due to secondary unfolding. The requirement of CSP-α to maintain proper protein folding in the mTOR pathway warrants further investigation. In addition, the CSP-α KO phenotype is comparable to the phenotype observed in the hippocampus upon conditional deletion of phosphatase and tensin homolog on chromosome 10 (PTEN) in postnatal/young adult neural stem cells (6, 43). PTEN is a negative regulator of PI3K signaling; therefore, its deletion leads to mTOR hyperactivation. Interestingly, PTEN-deleted adult neural stem cells display increased cell proliferation and depletion of the RGL pool. Our data indicate that, in the absence of CSP-α, RGL cell proliferation translates into a high number of intermediate progenitor cells (*SI Appendix*, Fig. S5), consistent with the notion that RGL cells differentiate toward a neural cell fate. We have also observed obvious alterations in the neuronal positioning of dividing progenitors at the SGZ (*SI Appendix*, Fig. S5), another feature previously known to occur upon mTOR hyperactivation as a consequence of the deletion of disrupted-in-schizophrenia 1 (DISC1) (49, 50). A very recent study has shown that autocrine signaling mediated by milk fat globule-EGF 8 (Mfge8) prevents developmental exhaustion of the adult neural stem cell pool (51). Remarkably, loss of Mfge8 promotes activation of RGLs and mTOR1 signaling that become rescued by rapamycin-mediated inhibition (51). Given the striking similarity of phenotypes related to mTOR hyperactivation in mice lacking CSP-α and mice lacking Mfge8, it would not be surprising that CSP-α could play a role within the signaling pathway mediated by this niche factor. This scenario certainly deserves to be further investigated. Overall, our data support a key connection of CSP-α with the maintenance of neural stem cell quiescence via a (likely) cell-autonomous mechanism dependent on the mTOR signaling pathway. A question that arises concerns the direct or indirect molecular relationship between CSP-α and the mTORC-dependent pathway that impacts neural stem cell proliferation. This question, which is beyond the scope of our data, remains unresolved. Nevertheless, an abbreviated explanation of our findings could be that CSP-α plays, within the IP3K/Akt/mTORC1 cascade, a regulatory role in key biochemical reactions that maintain quiescence under basal conditions. Such a role for CSP-α could involve the stabilization of specific proteins or protein complexes that require the cochaperone activity of CSP-α, as is required for SNARE complex stability (14, 15) or the polymerization of dynamin1 (28). In any case, although we do not have any evidence supporting the participation of signaling pathways besides the mTOR pathway, we cannot completely rule out that, additionally, other pathways could be involved in the phenotype we have described.

How do our results fit within the proposed role of CSP-α to maintain highly active synapses and to prevent neurodegeneration? Recent studies elegantly demonstrated the ability of neuronal circuitry mechanisms mediated by parvalbumin interneurons to control quiescence in hippocampal adult neural stem cells (8, 26). Certainly, during our study, we considered that the loss of quiescence in CSP-α KO mice could be a consequence of the presynaptic degeneration that GABAergic terminals in these mice suffer from (19). However, we can rule out that the early RGL cell hyperproliferation that we observe is caused by a lack of GABAergic input from parvalbumin-positive interneurons. At early postnatal ages, when neural stem cell hyperproliferation is clear, we could not detect obvious signs of GABAergic degeneration based on electrophysiological measurements of synaptic transmission (*SI Appendix*, Fig. S6). Furthermore, the phenotype observed in neurospheres is likely to be due to a cell-autonomous and not circuitry-dependent mechanism (Fig. 4 and *SI Appendix*, Fig. S6). This notion is, however, supported by the higher cell proliferation found in the *Sox2*^{CreERT2}:*Dnajc5*$^{flox/-}$ mice. Nonetheless, the fact that the synaptic competence of parvalbumin-positive interneurons progressively worsens in CSP-α KO mice suggests that, at some later stage, the postnatal neurogenesis will undergo circuit-dependent alterations in these mice. Future approaches will need to study this possibility at late postnatal ages using conditional ablation of CSP-α expression in parvalbumin-positive interneurons without compromising mouse viability.

CSP-α KO mice suffer from presynaptic degeneration and early lethality due to a severe neurological phenotype (18). In humans, mutations in the DNAJC5 gene that encodes CSP-α cause adult-onset neuronal ceroid lipofuscinosis (NCL4), a neurodegenerative disease with pathological features related to lysosomal storage disorders (22). Interestingly, lysosomes function as a scaffolding platform on which mTORC1 becomes activated. The Rag GTPases bring mTORC1 to the lysosomal surface in response to nutrients; once there, mTORC1 kinase activity is promoted by Rheb GTPase in response to insulin and energy levels (52). The details on how the high-molecular-weight protein complex mTORC1 swiftly docks on the Rag GTPases at the lysosomal surface are not well understood yet (52), and it would not be surprising if a cochaperone plays a role there. Remarkably, CSP-α has been found to be dynamically associated with the lysosome, depending on nutrient levels and the activation status of mTORC1 (53). Future experiments will investigate the molecular details between CSP-α and mTORC1 to support lysosomal function. Therefore, our study certainly opens interesting perspectives, beyond the alterations in neurogenesis, to understand the role of CSP-α in brain disorders and neurodegeneration. The mTOR pathway has been widely implicated in neurodegenerative disorders, particularly because mTORC hyperactivation exerts potent inhibition of autophagy (54), and a number of observations point to failures in autophagic degradation as a major culprit in neurodegeneration (55). Notwithstanding, much attention is being paid to rapamycin as a therapeutic option in the treatment of neurodegeneration (56). Therefore, the unexpected relationship between CSP-α and the mTOR signaling pathway that we have discovered undoubtedly opens unanticipated alternatives to explore mechanisms to understand and combat neurodegeneration.

Experimental Procedures

Mice. CSP-α KO (18), nestin-GFP (57) and conditional *Dnajc5* (CSP-α) KO mouse strains (described below) were used in this study. All procedures involving animals were performed in accordance with European Union Directive 2010/63/EU on the protection of animals used for scientific purposes and were approved by the Committee of Animal Use for Research at the University of Seville.

Generation of Conditional *Dnajc5* (CSP-α) KO Mice. Mice were generated from ES cells acquired from the European Conditional Mouse Mutagenesis Program. The mutant cells were generated by recombinant insertion of a KO first mutant construct (58) containing loxP sites flanking exon 3 of the mouse DNAJC5 gene (ENSMUSE00000170833 chromosome 2: 181282045–181282258). Chimeric mice were generated at the Animal Transgenic Unit of the Center of Animal Biotechnology and Gene Therapy, Universitat Autònoma de Barcelona, as described in *SI Appendix, SI Materials and Methods*.

Immunohistochemistry and Confocal Imaging. Tissue was obtained from control and CSP-α KO mice. An antigen retrieval protocol (modified from ref. 6) was used for nestin, Sox2, and MCM2 antibodies before an immunofluorescence protocol. Extended immunohistochemistry, acquisition, and image analysis protocols are explained in *SI Appendix, SI Materials and Methods*.

BrdU and EdU Labeling. BrdU (Sigma) was injected i.p. into CSP-α WT and KO mice, while EdU (BaseClick GmbH) was injected i.p. into *Sox2*^{CreERT2}:*Dnajc5*$^{flox/+}$ and *Sox2*^{CreERT2}:*Dnajc5*$^{flox/-}$ mice to perform proliferation assays. The protocols for immunolabeling BrdU and revealing EdU are explained in *SI Appendix, SI Materials and Methods*.

Other Methods. Procedures related to electrophysiology, neurosphere culture, flow cytometry, rapamycin treatment, protein biochemistry, and other methods are explained in detail in *SI Appendix, SI Materials and Methods*.

ACKNOWLEDGMENTS. We thank Thomas C. Südhof and María Luz Montesinos for critical reading of an early version of the manuscript and insightful comments; Lin Gao, José López-Barneo, Aixa Morales, Silvia K. Nicolis, Juan Galcerán, and Ángela M. Nieto for providing specific transgenic mouse strains; Alejandro Arroyo and Casandra Cabrera for excellent technical assistance; and staff members at research facilities located at Instituto de Biomedicina de Sevilla, the University of Seville School of Medicine, and Centro de Investigación, Tecnología e Innovación de la Universidad de Sevilla for technical support and advice. This work was supported by the Spanish Ministry of Economy and Competitiveness (MINECO) and Fondo Europeo de Desarrollo Regional (Grants BFU2013-47493-P and BFU2016-76050-P, Juan de la Cierva Contract, and Fellowships BES2008-002858 and BES2014-070405), the Junta de Andalucía (Grants P12-CTS-2232 and CTS-600), and the Instituto de Salud Carlos III. ES cells were acquired from the European Conditional Mouse Mutagenesis Program.

1. Altman J, Das GD (1965) Autoradiographic and histological evidence of postnatal hippocampal neurogenesis in rats. *J Comp Neurol* 124:319–335.
2. Nakashiba T, et al. (2012) Young dentate granule cells mediate pattern separation, whereas old granule cells facilitate pattern completion. *Cell* 149:188–201.
3. Clelland CD, et al. (2009) A functional role for adult hippocampal neurogenesis in spatial pattern separation. *Science* 325:210–213.
4. Akers KG, et al. (2014) Hippocampal neurogenesis regulates forgetting during adulthood and infancy. *Science* 344:598–602.
5. Christian KM, Song H, Ming GL (2014) Functions and dysfunctions of adult hippocampal neurogenesis. *Annu Rev Neurosci* 37:243–262.
6. Bonaguidi MA, et al. (2011) In vivo clonal analysis reveals self-renewing and multipotent adult neural stem cell characteristics. *Cell* 145:1142–1155.
7. Encinas JM, et al. (2011) Division-coupled astrocytic differentiation and age-related depletion of neural stem cells in the adult hippocampus. *Cell Stem Cell* 8:566–579.
8. Song J, et al. (2012) Neuronal circuitry mechanism regulating adult quiescent neural stem-cell fate decision. *Nature* 489:150–154.
9. Kempermann G, Chesler EJ, Lu L, Williams RW, Gage FH (2006) Natural variation and genetic covariance in adult hippocampal neurogenesis. *Proc Natl Acad Sci USA* 103:780–785.
10. Furutachi S, Matsumoto A, Nakayama KI, Gotoh Y (2013) p57 controls adult neural stem cell quiescence and modulates the pace of lifelong neurogenesis. *EMBO J* 32:970–981.
11. Zou P, et al. (2011) p57(Kip2) and p27(Kip1) cooperate to maintain hematopoietic stem cell quiescence through interactions with Hsc70. *Cell Stem Cell* 9:247–261.
12. Ramírez-Rodríguez G, et al. (2013) The α crystallin domain of small heat shock protein b8 (Hspb8) acts as survival and differentiation factor in adult hippocampal neurogenesis. *J Neurosci* 33:5785–5796.
13. Tobaben S, et al. (2001) A trimeric protein complex functions as a synaptic chaperone machine. *Neuron* 31:987–999.
14. Chandra S, Gallardo G, Fernández-Chacón R, Schlüter OM, Südhof TC (2005) Alpha-synuclein cooperates with CSPalpha in preventing neurodegeneration. *Cell* 123:383–396.
15. Sharma M, Burré J, Südhof TC (2011) CSPα promotes SNARE-complex assembly by chaperoning SNAP-25 during synaptic activity. *Nat Cell Biol* 13:30–39.
16. Rozas JL, et al. (2012) Motorneurons require cysteine string protein-α to maintain the readily releasable vesicular pool and synaptic vesicle recycling. *Neuron* 74:151–165.
17. Sharma M, Burré J, Südhof TC (2012) Proteasome inhibition alleviates SNARE-dependent neurodegeneration. *Sci Transl Med* 4:147ra113.
18. Fernández-Chacón R, et al. (2004) The synaptic vesicle protein CSP alpha prevents presynaptic degeneration. *Neuron* 42:237–251.
19. García-Junco-Clemente P, et al. (2010) Cysteine string protein-alpha prevents activity-dependent degeneration in GABAergic synapses. *J Neurosci* 30:7377–7391.
20. Sharma M, et al. (2012) CSPα knockout causes neurodegeneration by impairing SNAP-25 function. *EMBO J* 31:829–841.
21. Valenzuela-Villatoro M, García-Junco-Clemente P, Nieto-González JL, Fernández-Chacón R (2018) Presynaptic neurodegeneration: CSP-α/DNAJC5 at the synaptic vesicle cycle and beyond. *Curr Opin Physiol* 4:65–69.
22. Nosková L, et al. (2011) Mutations in DNAJC5, encoding cysteine-string protein alpha, cause autosomal-dominant adult-onset neuronal ceroid lipofuscinosis. *Am J Hum Genet* 89:241–252.
23. Chamberlain LH, Burgoyne RD (1996) Identification of a novel cysteine string protein variant and expression of cysteine string proteins in non-neuronal cells. *J Biol Chem* 271:7320–7323.
24. Kohan SA, et al. (1995) Cysteine string protein immunoreactivity in the nervous system and adrenal gland of rat. *J Neurosci* 15:6230–6238.
25. Enikolopov G, Overstreet-Wadiche L (2008) The use of reporter mouse lines to study adult neurogenesis. *Adult Neurogenesis*, eds Fred H, Gage K, Hongjun S (Cold Spring Harbor Laboratory Press, Cold Spring Harbor, NY), pp 81–100.
26. Song J, et al. (2013) Parvalbumin interneurons mediate neuronal circuitry-neurogenesis coupling in the adult hippocampus. *Nat Neurosci* 16:1728–1730.
27. Leshchyns'ka I, et al. (2006) The adhesion molecule CHL1 regulates uncoating of clathrin-coated synaptic vesicles. *Neuron* 52:1011–1025.
28. Zhang YQ, et al. (2012) Identification of CSPα clients reveals a role in dynamin 1 regulation. *Neuron* 74:136–150.
29. Andreu Z, et al. (2015) The cyclin-dependent kinase inhibitor p27 kip1 regulates radial stem cell quiescence and neurogenesis in the adult hippocampus. *Stem Cells* 33:219–229.
30. Lie DC, et al. (2005) Wnt signalling regulates adult hippocampal neurogenesis. *Nature* 437:1370–1375.
31. Imayoshi I, Sakamoto M, Yamaguchi M, Mori K, Kageyama R (2010) Essential roles of Notch signaling in maintenance of neural stem cells in developing and adult brains. *J Neurosci* 30:3489–3498.
32. Lai K, Kaspar BK, Gage FH, Schaffer DV (2003) Sonic hedgehog regulates adult neural progenitor proliferation in vitro and in vivo. *Nat Neurosci* 6:21–27.
33. Aberg MA, et al. (2003) IGF-I has a direct proliferative effect in adult hippocampal progenitor cells. *Mol Cell Neurosci* 24:23–40.
34. Fingar DC, et al. (2004) mTOR controls cell cycle progression through its cell growth effectors S6K1 and 4E-BP1/eukaryotic translation initiation factor 4E. *Mol Cell Biol* 24:200–216.
35. Favaro R, et al. (2009) Hippocampal development and neural stem cell maintenance require Sox2-dependent regulation of Shh. *Nat Neurosci* 12:1248–1256.
36. Rotheneichner P, et al. (2017) Tamoxifen activation of Cre-recombinase has No persisting effects on adult neurogenesis or learning and anxiety. *Front Neurosci* 11:27.
37. Shin J, et al. (2015) Single-cell RNA-seq with waterfall reveals molecular cascades underlying adult neurogenesis. *Cell Stem Cell* 17:360–372.
38. Dulken BW, Leeman DS, Boutet SC, Hebestreit K, Brunet A (2017) Single-cell transcriptomic analysis defines heterogeneity and transcriptional dynamics in the adult neural stem cell lineage. *Cell Rep* 18:777–790.
39. Hochgerner H, Zeisel A, Lönnerberg P, Linnarsson S (2018) Conserved properties of dentate gyrus neurogenesis across postnatal development revealed by single-cell RNA sequencing. *Nat Neurosci* 21:290–299.
40. Melo-Braga MN, et al. (2014) Comprehensive quantitative comparison of the membrane proteome, phosphoproteome, and sialiome of human embryonic and neural stem cells. *Mol Cell Proteomics* 13:311–328.
41. Magri L, et al. (2011) Sustained activation of mTOR pathway in embryonic neural stem cells leads to development of tuberous sclerosis complex-associated lesions. *Cell Stem Cell* 9:447–462.
42. Rodgers JT, et al. (2014) mTORC1 controls the adaptive transition of quiescent stem cells from G0 to G(Alert). *Nature* 510:393–396.
43. Amiri A, et al. (2012) Pten deletion in adult hippocampal neural stem/progenitor cells causes cellular abnormalities and alters neurogenesis. *J Neurosci* 32:5880–5890.
44. Paliouras GN, et al. (2012) Mammalian target of rapamycin signaling is a key regulator of the transit-amplifying progenitor pool in the adult and aging forebrain. *J Neurosci* 32:15012–15026.
45. Gan B, et al. (2008) mTORC1-dependent and -independent regulation of stem cell renewal, differentiation, and mobilization. *Proc Natl Acad Sci USA* 105:19384–19389.
46. Castilho RM, Squarize CH, Chodosh LA, Williams BO, Gutkind JS (2009) mTOR mediates Wnt-induced epidermal stem cell exhaustion and aging. *Cell Stem Cell* 5:279–289.
47. Nellist M, Burgers PC, van den Ouweland AM, Halley DJ, Luider TM (2005) Phosphorylation and binding partner analysis of the TSC1-TSC2 complex. *Biochem Biophys Res Commun* 333:818–826.
48. Nellist M, et al. (2005) Distinct effects of single amino-acid changes to tuberin on the function of the tuberin-hamartin complex. *Eur J Hum Genet* 13:59–68.
49. Duan X, et al. (2007) Disrupted-In-Schizophrenia 1 regulates integration of newly generated neurons in the adult brain. *Cell* 130:1146–1158.
50. Kim JY, et al. (2009) DISC1 regulates new neuron development in the adult brain via modulation of AKT-mTOR signaling through KIAA1212. *Neuron* 63:761–773.
51. Zhou Y, et al. (2018) Autocrine Mfge8 signaling prevents developmental exhaustion of the adult neural stem cell pool. *Cell Stem Cell* 23:444–452.e4.
52. Sabatini DM (2017) Twenty-five years of mTOR: Uncovering the link from nutrients to growth. *Proc Natl Acad Sci USA* 114:11818–11825.
53. Wyant GA, et al. (2018) NUFIP1 is a ribosome receptor for starvation-induced ribophagy. *Science* 360:751–758.
54. Menzies FM, Fleming A, Rubinsztein DC (2015) Compromised autophagy and neurodegenerative diseases. *Nat Rev Neurosci* 16:345–357.
55. Wong E, Cuervo AM (2010) Autophagy gone awry in neurodegenerative diseases. *Nat Neurosci* 13:805–811.
56. Bové J, Martínez-Vicente M, Vila M (2011) Fighting neurodegeneration with rapamycin: Mechanistic insights. *Nat Rev Neurosci* 12:437–452.
57. Mignone JL, Kukekov V, Chiang AS, Steindler D, Enikolopov G (2004) Neural stem and progenitor cells in nestin-GFP transgenic mice. *J Comp Neurol* 469:311–324.
58. Skarnes WC, et al. (2011) A conditional knockout resource for the genome-wide study of mouse gene function. *Nature* 474:337–342.